Control over the Self-Assembly Modes of Pt(II) Complexes by Alkyl Chain Variation: From Slipped to Parallel π-Stacks

Naveen Kumar Allampally,[†] María José Mayoral,[†,#] Sarayute Chansai,[‡] María Cristina Lagunas,[‡] Christopher Hardacre,[‡] Vladimir Stepanenko,[†] Rodrigo Q. Albuquerque[¥] and Gustavo Fernández[*†§]

† Institut für Organische Chemie and Center for Nanosystems Chemistry, Universität Würzburg Am Hubland, 97074 Würzburg, Germany

‡ School of Chemistry and Chemical Engineering, Queen's Universtity Belfast, Stranmillis Road, Belfast BT9 5AG, United Kingdom

¥ São Carlos Institute of Chemistry, University of São Paulo, Av. Trab. São-Carlense, 400, 13560-970 São Carlos-SP, Brazil

ABSTRACT: We report the self-assembly of a new family of hydrophobic, bis(pyridyl) Pt(II) complexes featuring an extended OPE-derived π-surface appended with six long (dodecyloxy (**2**)) or short (methoxy (**3**)) side groups. Complex **2** containing dodecyloxy chains forms fibrous assemblies with a slipped arrangement of the monomer units ($d_{Pt\cdots Pt} \approx 14$ Å) in nonpolar solvents and the solid state. Dispersion-corrected PM6 calculations suggest that this organization is driven by cooperative π–π, C-H···Cl and π-Pt interactions, which is supported by EXAFS and 2D NMR. In contrast, nearly parallel π-stacks ($d_{Pt\cdots Pt} \approx 4.4$ Å) stabilized by multiple π–π and C-H···Cl contacts are obtained in the crystalline state for **3** lacking long side chains, as shown by X-Ray and PM6. Our results reveal not only the key role of alkyl chain length in controlling self-assembly modes but also the relevance of Pt-bound chlorine ligands as new supramolecular synthons.

1. INTRODUCTION

Understanding the non-covalent forces that govern the formation of self-assembled structures and in particular supramolecular polymers,[1-4] is a prerequisite to construct functional materials, being optoelectronics and biomedicine two of the most prosperous research fields in this regard.[5-17] In order to achieve these functionalities, highly-ordered, adaptive nanostructures formed via a cooperative supramolecular polymerization mechanism are highly desirable.[18] The introduction of orthogonal non-covalent interactions,[19] from which hydrogen bonding and combinations with other secondary interactions are by far the most exploited ones,[20] represents a rational means for this purpose. The majority of these systems include purely organic building blocks, whereas the role of metal ions and polarized metal-bound atoms has been explored to a much lesser extent.

Square-planar Pt(II) compounds are particularly relevant systems in this context due to their exceptional physicochemical, redox, catalytic, anticancer and supramolecular properties.[21-30] These systems have a strong propensity to aggregate in solution and in the solid state via Pt···Pt and/or other secondary forces, as recently shown for various classes of complexes in a comprehensive review by Yam and co-workers.[31] Among them, the self-assembly features of hydrophobic Pt(II) complexes with acetylide,[32-36] bidentate,[37-39] tridentate N-donor,[40-42] and cyclometalating ligands[43-45] are relatively well understood.[31] In contrast, their hydrophobic counterparts featuring non-chelating ligands and, in particular, bis(pyridyl) Pt(II) complexes have been limited to liquid crystalline materials[46-48] and hydrogen-bonded metallogelators.[49,50] Thus, there is a need for a deeper understanding of this class of Pt(II) complexes, in which not only the nature of the metal ion but also a wide range of weak unconventional forces stemming from the ligands attached to the metal fragment[51,52] anticipate the discovery of new supramolecular synthons.

In this article, we report a new family of hydrophobic bis(pyridyl)dichloride Pt(II) complexes exhibiting a large aromatic oligophenyleneethynylene (OPE)-based platform and peripheral dodecyloxy (**2**) and methoxy (**3**) chains. The remarkably different molecular arrangement of **2** and **3** brings to light that the alkyl chain length plays an important role in the self-assembly, inducing the participation of various unconventional non-covalent forces. This has been demonstrated by a battery of experimental methods, including temperature-dependent UV-Vis and ^{1}H NMR, ROESY NMR, atomic force microscopy (AFM), scanning electron microscopy (SEM), wide angle X-ray scattering (WAXS), extended X-Ray absorption fine structure (EXAFS), X-Ray diffraction and dispersion-corrected PM6 quantum chemical calculations. In nonpolar solvents, slipped π-stacks driven by cooperative π–π, C-

H···Cl and π-Pt contacts are formed for **2**, whereas nearly parallel stacks with Pt···Pt distances of 4.4 Å are obtained in the crystal structure of **3**. In contrast to previously reported structurally related bis(pyridyl)dichloride Pd(II) complexes,[53] our studies demonstrate that not only the presence or absence of peripheral chains but also the nature of the metal ion (Pt(II)) is responsible for the rearrangement of the molecules into various packing modes.

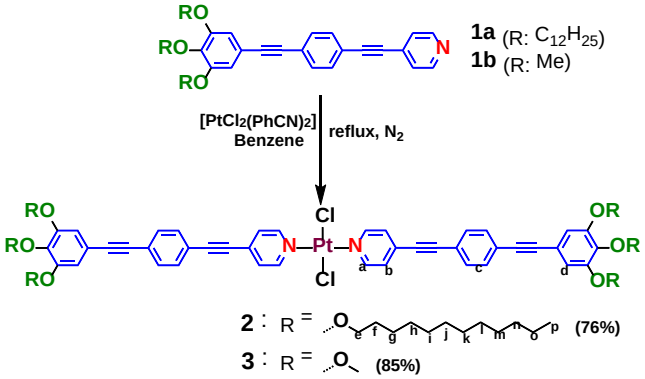

Scheme 1. Synthetic route to obtain Pt(II) complexes **2** and **3**.

2. Results and Discussion

OPE-based pyridyl ligand **1a** featuring dodecyloxy chains has been previously synthesized according to literature procedures[53] whereas its homologue with shorter methoxy groups (**1b**) has been obtained by a sequence of cross-coupling reactions and selective deprotection protocols (see Supporting Information (SI)). The target OPE-based Pt(II) complexes **2**-**3** have been successfully obtained in very good yields by refluxing a mixture of **1a**-**b** (2 eq.) and $Pt(PhCN)_2Cl_2$ (1 eq.) in dry benzene for 2-3 days under N_2 gas. **2** and **3** have been well characterized by NMR, HRMS, IR, elemental analyses and X-Ray diffraction (for **3**) (see further details in the SI).

UV-Vis measurements of **2** were recorded in solvents of different polarity (THF, $CHCl_3$, dichloromethane (DCM), cyclohexane (CHY) and methylcyclohexane (MCH)) in order to observe the solvent dependency of the spectra (Figure 1a and S1). In all solvents at a concentration of ≈9 × 10^{-6} M, **2** shows two transitions with maxima at 285 nm and 360 nm. The former can be assigned to a typical ligand centered transition (^{1}LC, π–π*, 275-315 nm) whereas the latter is due to metal to ligand charge transfer (^{1}MLCT, 320 - 380 nm).[54] Intriguingly, there is no particular effect of the polarity of the solvent on the absorption maxima at this concentration in the investigated solvents. An increase in concentration to 1 × 10^{-4} M does not lead to significant spectral changes with the exception of MCH, in which noticeable spectral changes in the course of temperature-dependent experiments at a concentration of 5 × 10^{-5} M are observed. The maximum red-shifts from 360 to 377 nm, while a new sharp transition rises around 410 nm on varying the temperature from 340 to 273 K (Figure 1a and S2). This particular phenomenon suggests that aggregation does occur and we have observed that it is thermally reversible. Thus, **2** still exists as monomeric state in THF, $CHCl_3$ and CH_2Cl_2 even at higher concentrations (good solvents), whereas as self-assembled species in MCH (hydrophobic solvent). To confirm that the red shifted band at 377 nm and the sharp shoulder at ≈410 nm are due to aggregation, we have prepared thin films from CH_2Cl_2 and MCH. The UV-Vis spectrum of a thin film from CH_2Cl_2 shows the representative spectral features of a molecularly dissolved state, i.e. an absorption maximum at ≈360 nm (Figure S1). The position of this maximum matches well that observed in MCH at high temperatures. In sharp contrast and similarly to the behavior in MCH solution at low temperatures, the thin film from MCH presents a red shifted aggregate band at 377 nm along with a new shoulder at 400 nm, confirming the formation of self-assembled species in this medium (Figure S1).

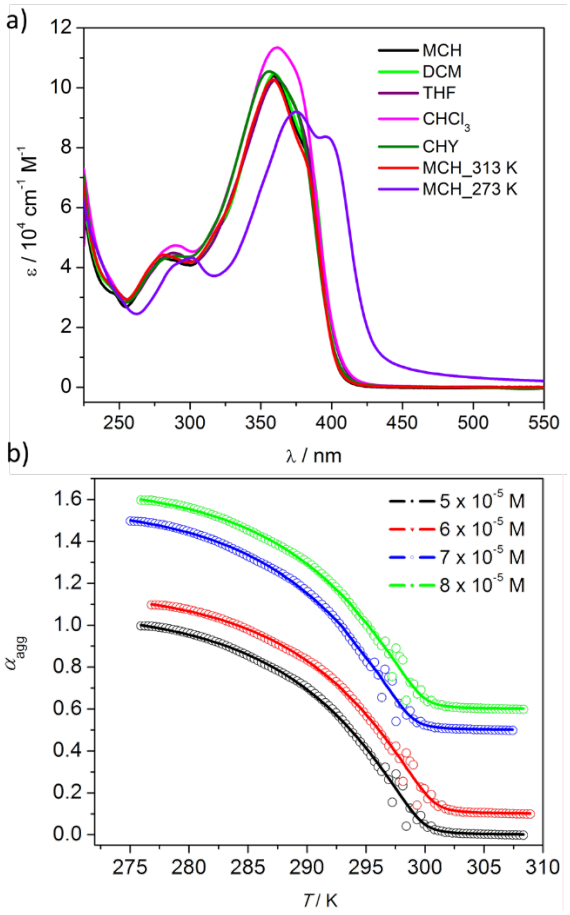

Figure 1. a) Absorption spectra of **2** in various solvents (9 × 10^{-6} M) at r.t. and in MCH (conc. 5 × 10^{-5} M) at two different temperatures (358 K (red) and 283 K (purple)). b) Cooling curves at different concentrations of **2** in MCH, fitting of α_{agg} vs. T in the framework of the ten Eikelder-Markvoort-Meijer model. The red, blue and green curves have been slightly shifted for better visualization.

In order to closely follow the self-assembly process in MCH solution, we have monitored the spectral changes at a given wavelength (400 nm) by slowly cooling down

MCH solutions (conc. 5 - 8 × 10^{-5} M) of **2** from 323 to 274 K. To verify that the self-assembly progresses under thermodynamic control, a cooling rate of 1 K/min has been chosen. A particularly interesting temperature range of the self-assembly process is 315-276 K, where a clear transition from monomeric to aggregated species is observed, yielding non-sigmoidal cooling curves (see Figure 1b).

Table 1. Thermodynamic parameters associated to the self-assembly of 2 at different concentrations.

Conc. M	$\Delta H°_{nucl}$ kJmol^{-1}	$\Delta H°$ kJmol^{-1}	$\Delta S°$ kJmol^{-1}K^{-1}	T_e K	K_2 M^{-1}	K M^{-1}	σ
5 × 10^{-4}	-17.4 ± 0.3	-81.4 ± 0.5	-0.1898 ± 0.0017	299.1 ± 0.05	20.2	2.25 × 10^4	8.9 × 10^{-4}
6 × 10^{-4}	-17.5 ± 0.2	-90.5 ± 0.2	-0.2215 ± 0.0007	299.4 ± 0.03	16.9	1.97 × 10^4	8.6 × 10^{-4}
7 × 10^{-4}	-19.3 ± 0.1	-92.9 ± 0.2	-0.2303 ± 0.0006	300.0 ± 0.02	7.5	1.81 × 10^4	4.2 × 10^{-4}
8 × 10^{-4}	-20.4 ± 0.1	-100.2 ± 0.2	-0.2550 ± 0.0005	300.6 ± 0.02	4.7	1.77 × 10^4	2.6 × 10^{-4}
Global[a] fitting	-12.5 ± 0.5	-117.4 ± 2.7	-0.3130 ± 0.0091	298.4[c]	103.9	1.57 × 10^4	6.6 × 10^{-3}
Global[b] fitting	-12.2 ± 0.5	-119.7 ± 2.7	-0.3207 ± 0.0091	298.4[c]	113.4	1.55 × 10^4	7.3 × 10^{-3}

[a] Normalize data with single normalization constant; [b] Normalize each curve individually; [c] average value.

Further to calculate the thermodynamic parameters, the obtained cooling curves are fitted to the ten Eikelder-Markvoort-Meijer model,[55,56] confirming that the self-assembly mechanism of **2** is a highly cooperative phenomenon (Figure 1b and S2). The corresponding thermodynamic parameters are displayed in Table 1. This model assumes that nuclei of two molecules of **2** are formed in the first unfavorable nucleation step followed by a much more favorable elongation into supramolecular polymeric nanostructures. According to the thermodynamic analysis, the dimerization constants (K_d) range from 4.7 to 20.2 M^{-1} while the elongation constants (K_e) are around 1000-fold higher (1.77-2.25 × 10^4 M). The quotient between the nucleation and elongation constants yields low values of σ (2.6-8.9 × 10^{-4}), which denote a high degree of cooperativity (for a global analysis of the fits see Table 1, bottom). By comparing these thermodynamic parameters with those calculated for a structurally related OPE-based bis(pyridyl)dichloride Pd(II) investigated in our group,[53] slight differences can be noticed. For instance, the K_d for Pt(II) complex **2** is approximately two orders of magnitude higher (≈0.65 vs. ≈100 M^{-1}) while the K_e is around three times higher (≈7.7 × 10^3 vs. ≈2 × 10^4 M^{-1}) than those obtained for the analogous Pd(II) derivative. This demonstrates that the nature of the metal ion plays a role in the self-assembly and degree of cooperativity.

As the self-assembly process is observed to be cooperative, the aggregate growth should be governed by the interplay of various orthogonal non-covalent interactions.[19] The presence of an extended aromatic surface in **2** anticipates that strong π–π interactions will be a major contribution to the supramolecular polymerization. According to literature precedent, we hypothesized that either metal···metal[53] or weak interactions[52] involving the Cl-Pt(II)-Cl fragment of **2** could represent additional forces to the cooperative growth. In order to find this out, we have performed temperature-dependent ^{1}H NMR and 2D-NMR in MCH-d_{14}. Variable-temperature ^{1}H NMR studies (8 mM, 400 MHz, 351-308 K) show a slight upfield shift of most aromatic signals with decreasing temperature, in particular those corresponding to the H_a protons of the pyridine rings, suggesting that π-stacking interactions are involved in the self-assembly process (Figure S3).

By comparing the COSY and ROESY spectra (Figure S3-S4), we found new cross-peaks in the latter experiments that can be assigned to the coupling of some of the protons of the phenylene rings in the aggregate structure. Interestingly, protons H_d of the outer ring are coupling with protons H_a and H_b of the pyridine units (Figure 2a), which is also predicted by theoretical calculations (vide infra). The appearance of these signals confirms that the units of **2** cannot be arranged into parallel stacks *via* π–π and Pt···Pt interactions, as the intermolecular distance between protons H_a and H_d (≈13 Å) would be much larger than the estimated distance (≤ 5 Å) for nuclear spins to correlate. The results extracted from both 1D and 2D NMR experiments for **2** closely resemble those obtained for analogous amphiphilic Pt(II) complexes investigated in our group.[52] For these systems, the presence of polar glycol side chains induces a translational displacement of the OPE scaffolds within the supramolecular fiber driven by CH···O and CH···Cl weak hydrogen bonding involving the oxygen and hydrogen atoms of the polar chains. Thus, in the light of these results it appears that the hydrophobic Pt(II) complex **2** self-assembles in a similar fashion into slipped π-stacks in MCH solution despite the absence of multiple polarizable oxygen atoms in the side chains. As a result, other secondary forces apart from π–π interactions should be necessarily involved to stabilize the stack, most likely interactions involving the Cl-Pt(II)-Cl fragments and the aromatic rings of adjacent molecules.

To analyse the possible non-covalent interactions that help maintain the slipped packing of **2** deduced by 2D NMR studies, we have performed quantum chemical calculations at the PM6 semiempirical level with dispersion corrections[57] using the MOPAC program.[58,59] The optimized geometry of a tetramer of **2** is shown in Figure 2b, where hydrogens were omitted for clarity. It is clear how intermolecular van der Waals interactions among alkyl chains contribute to stabilize the stack. Aromatic interactions are also important here: four out of six aromatic rings of each monomer participate in such contacts. Intermolecular interactions between outer aromatic rings

and alkyl chains (CH···π) are also observed in Figure 2b, where many pairs of alkyl protons-H_a protons (see Scheme 1 for proton labeling) have distances smaller than 5 Å. This is in agreement with the correlation between most protons of the alkyl chains ($H_{e\text{-}g}$) and aromatic protons $H_{a\text{-}d}$ obtained in the ROESY spectra (Figure S3). The intramolecular (H_c···H_d and H_b···H_c) and intermolecular (H_a···H_c and H_b···H_c) distances obtained from the optimized tetramer are also smaller than 5 Å, which agrees well with the ROESY signals found (Figure 2a). Heats of formation predicted from the PM6 calculations for aggregates of **2** with different numbers (n) of monomer units (n = 1-4) were used to estimate the following ΔH values (in kJ/mol) of monomer addition: -255 (1+1→2), -352 (2+1→3), and -377 (3+1→4) (Figure S5). These values suggest that subsequent monomer additions become increasingly more stable for longer aggregates, which is in line with the cooperativity experimentally observed.

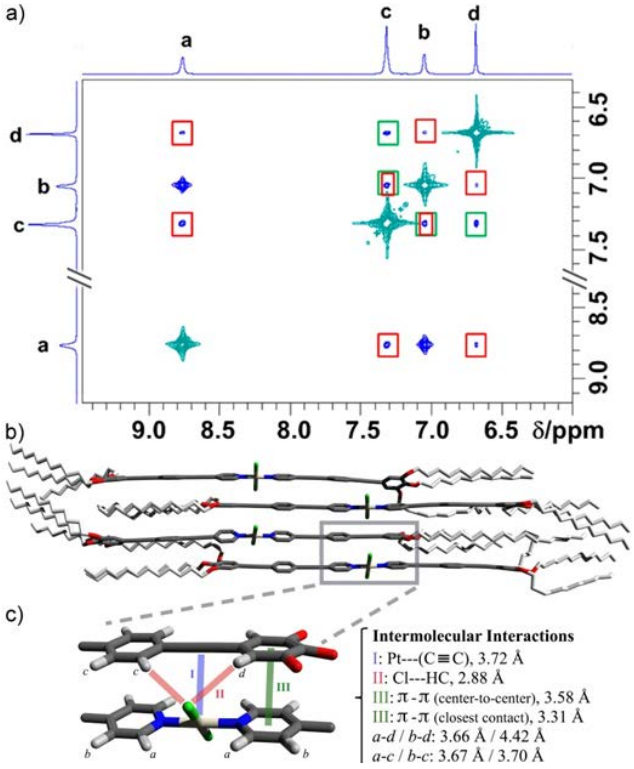

Figure 2. a) Partial ROESY NMR spectrum (MCH-d_{14}, 600 MHz, 8.73 mM, 305 K) of **2**. The green and red squares highlight intra- and intermolecular through-space coupling signals, respectively. b) PM6 geometry-optimized structure of a tetramer of **2**. c) Enlarged section of the structure depicted in (b) showing the most relevant non-covalent interactions.

Figure 2c shows a zoomed region of the optimized tetramer revealing different kinds of intermolecular interactions involving Cl, Pt, H-C and aromatic moieties. Protons $H_{a\text{-}d}$ are also labeled to show their close relative proximity, which explains why their 2D NMR signals are coupled (Figure 2a). The semiempirical calculations suggest that the slipped stacking depicted in Figure 2b is promptly destabilized if the alkyl chains are removed, i.e., if we use **3** instead of **2** to build the same stack. The optimized geometry of an octamer of **3** built in the slipped arrangement evidences that outer aromatic rings of the first and third (or second and fourth, etc) monomers in the stack would be strongly distorted to interact with each other (Figure S6). This distortion hampers further growth of the aggregate in the slipped arrangement, which nicely points out that the alkyl chains play a key role in the final arrangement of the supramolecular aggregate: the long side groups of **2** favor the slipped arrangement while the much shorter ones of **3** appear to destabilize it (vide infra).

Due to its hydrophobic character, **2** has a strong propensity to gel various hydrophobic solvents such as hexane, isooctane, dodecane and MCH in a reversible manner for various cycles (see SI). Their respective critical gelation concentrations (CGC) were observed to decrease upon increasing the chain length of the solvent, confirming that the gelation capacity of solvents containing shorter hydrocarbon chains is less effective. The surface morphology of the gels has been investigated by means of SEM and AFM. The respective SEM and AFM images of xerogels displayed in Figures 3 and S7 confirm that the surface morphology is not significantly affected by the solvent. The length of the fibers is in the order of μm and the width ranges from 50 to 100 nm. WAXS studies of a gel of **2** in hexane display a reflection at $2\theta = 26.8°$ that corresponds to a π–π distance of 3.3 Å between the units of **2** (Figure S7), in agreement with the values predicted by PM6 calculations.

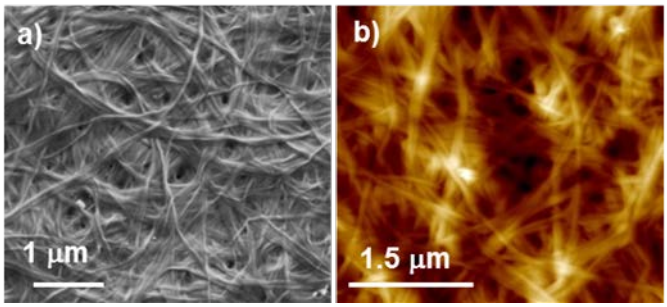

Figure 3. Surface morphology of xerogels of **2**. (a) SEM image from a gel in isooctane. (b) AFM of a dodecane gel on silicon wafer.

To rationalize the influence of the alkyl side groups on the self-assembly of **2**, we have investigated the analogous Pt(II) complex **3** lacking the dodecyloxy chains by X-Ray diffraction. The removal of these chains facilitates substantially the realization of single crystals in contrast to **2**, in which the presence of six long side groups cause a significant disorder in the crystal lattice. Nevertheless, the limited solubility of this complex in highly nonpolar solvents such as MCH precludes a detailed analysis of the supramolecular polymerization mechanism. Suitable crystals of **3** for X-ray analysis were obtained by slow evaporation from a concentrated solution (≈1 mM) of CH_3CN and CH_2Cl_2 (1:1). Figure 4 shows the molecular arrangement of **3** in the crystal structure in four different views. Within the monomeric units of **3**, the OPE-based ligands are nearly coplanar whereas the chlorine atoms attached to the Pt(II) ion are slightly bent out of the plane to facilitate interactions with neighbouring units of **3**

(Figure 4a). This slightly distorted square-planar coordination is stabilized by two intramolecular C-H···Cl interactions (2.919 and 2.869 Å) between the H_a of the pyridine rings and the chlorine atoms of the same molecule (Figure S9). The packing of **3** in the crystal structure is primarily driven by intermolecular C-H(aromatic)···Cl and translationally stacked π–π interactions, as the relatively bulky chlorine atoms hinder the alignment of the units of **3** in a perfect parallel fashion through Pt···Pt bonding. Each chlorine atom is involved in three intermolecular (py)CH···Cl interactions with two neighbouring monomers belonging to a parallel 1D stack (d = 3.09 and 2.79 Å) and to one monomer inside the same stack (d = 2.76 Å, Fig. S9). The three CH···Cl intermolecular contacts together with multiple π–π interactions (3.3 Å) involving the aromatic OPE rings facilitate the growth of the structure into 1D stacks (Figure 4a) and are responsible for the packing of the molecules as shown in Figures 4b-d. The molecular arrangement of **3** extracted from X-ray studies (Figure 4) is remarkably different when compared with that of **2** in MCH solution suggested by 2D NMR studies and theoretical calculations (Figure 2c), although for both systems the chlorine ligands are very important to stabilize the aggregates. Whereas **2** forms slipped stacks with ($d_{Pt\cdots Pt}$ ≈ 14 Å), the removal of the long chains in **3** enables a tighter molecular arrangement into almost parallel stacks with much shorter distances between the Pt centers (4.4 Å). It is important to note that the Pt···(C≡C) interaction is exclusively found in aggregates of **2** and it can involve σ and π electron donations to Pt, as well as δ and π back-donations. This interaction can contribute to a certain extent to the stabilization of the slipped configuration found for **2**, even though the PM6-predicted Pt---(C≡C) bond distances are larger than those usually found in Pt(II)-alkyne complexes. Although the molecular packing within a self-assembled structure and in the crystal state sometimes differ, our results bring to light that the presence of flexible alkyl chains in **2** represents a major contribution to shifting the packing in solution, as already pointed out by the theoretical calculations.

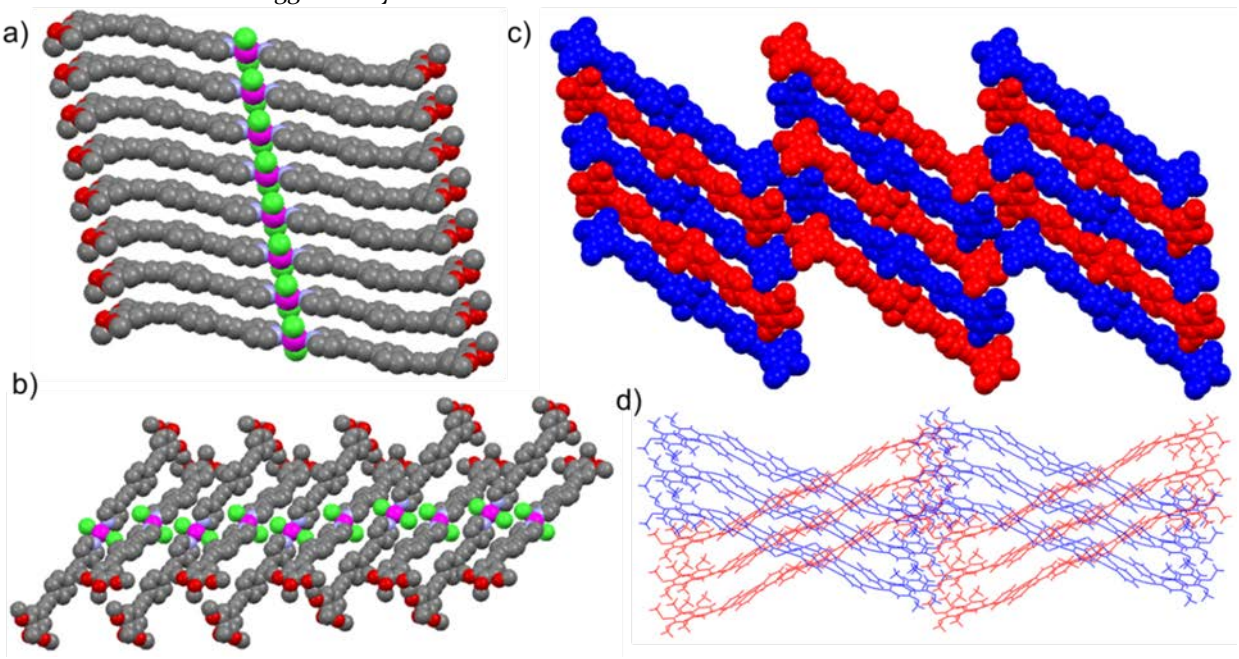

Figure 4. Arrangement of **3** in the crystal structure, a) vertical and b) horizontal views and c) 2D and d) 3D-Packing. The hydrogens have been omitted for clarity. Colour codes: Pt: pink; Cl: green; O: red; N: light blue; C. grey

Pt L_{III} extended EXAFS studies have been performed to further support the supramolecular assembly of **2** and establish a correlation between the solid-state packing and solution/gel of **2** in both hexane and MCH. k^3-weighted EXAFS spectra and Fourier Transforms (FTs) for the three samples are shown in Figure S10. The theoretical models for the EXAFS were constructed using crystallographic data from complex **3**, as well as from an analogous compound with unsubstituted pyridine ligands $[PtCl_2(py)_2]$.[60] The latter was chosen in order to reproduce the slipped molecular arrangement proposed for complex **2** (see Figure 2), in contrast to the almost parallel stacks with relatively short Pt···Pt distances (4.4 Å) observed in **3**. In particular, in the crystal packing of $[PtCl_2(py)_2]$, the molecules are organised in a such a way that two of the pyridine C atoms of one molecule are close to the Pt centre of the adjacent molecule (ca. 3.6 Å, see Figure S10). Details of EXAFS data analysis and of the scattering paths included in the theoretical models are provided in the SI (Tables S2-S5; Figures S11-S13).

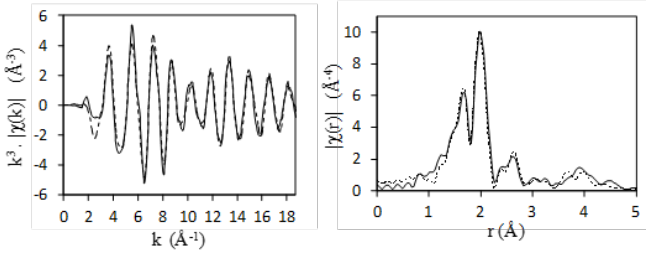

Figure 5. Data (solid line) and best-fit model (dotted line) for complex **2** in the solid state: k^3-Weighted EXAFS spectra (left) and magnitude of Fourier transform (right).

Figure 5 shows data and best-fit model for the EXAFS spectrum and FT for complex **2** in the solid state. Structural information extracted from the EXAFS fittings is included in Table S3. The two main features in the FT at ca. 1.6 Å and 2 Å (Figure 5) correspond to single scatterings from the N and Cl atoms, respectively, whereas the next peaks at 2.3-2.8 Å correspond mainly to contributions of the pyridine *ortho*-C atoms (single and multiple scattering paths). The smaller features between 2.8 and 3.5 Å can be best fitted by including multiple scattering paths Pt→N→Cl and Pt→N→N.

At this stage, the effect on the fitting of including contributions from other scattering paths from complex **3** and/or $[PtCl_2(py)_2]$ was carefully considered. The best-fit was obtained by including additional scattering paths only from $[PtCl_2(py)_2]$, in particular single and multiple scatterings involving the C atoms at 3.6 Å of adjacent molecules (*adj*-C) and the pyridine *meta*-C atoms. These paths contributed to the FT of the data in the region between 3.5-4.5 Å. Inclusion of additional or alternative scattering paths did not make a significant difference in the fitting. Particularly, if Pt→Pt and Pt→*meta*-C single scattering paths from complex **3** are considered instead of the C contributions from $[PtCl_2(py)_2]$, the fit worsens. These results support the molecular aggregation deduced by 2D NMR and quantum chemical calculations for complex **2** in solution, as discussed above. It should be noted that the Pt-adj-C distance determined by EXAFS for complex **2** (3.95±0.02 Å) is longer than that in the crystal structure of $[PtCl_2(py)_2]$ (3.6 Å), and can be related to the bulky pyridine substituents in **2**.

The EXAFS data for the gels in both hexane and MCH were then fitted applying the same parameters used in the best-fit model for the solid sample. The results obtained were analogous to those of the solid, with the best-fit achieved when using scattering from from Pt→*adj*C, thus suggesting that the molecules in both gels aggregate in the same way as in the solid sample (Figures S12-S13, Tables S4-S5).

3. Conclusions

The self-assembly of a new family of hydrophobic π-conjugated (bis)pyridyl Pt(II) complexes equipped with long (dodecyloxy, **2**) or short (methoxy, **3**) side groups is described. A collection of experimental and theoretical results shows remarkable differences in the self-assembly modes depending on the alkyl group length. Whereas Pt(II) complex **2** with long chains self-assembles into slipped π-stacks, the removal of the side groups in **3** enables a nearly parallel molecular arrangement with Pt···Pt distances of 4.4 Å. NMR studies, X-Ray, EXAFS and PM6 calculations have given insight on the multiple intermolecular interactions (π–π, Cl···H, Pt···π) involved in both arrangements. For both complexes, the Cl atoms have revealed to be fundamental to explain the driving force behind the self-assembly of **2** and **3**. Our findings show: 1) the key role of alkyl groups in controlling self-assembly modes and 2) the establishment of metal-bound Cl atoms as new synthon in the field of supramolecular chemistry.

ASSOCIATED CONTENT

Supporting Information: Synthesis and characterization, additional UV-Vis studies, cooling curves, 1D and 2D NMR, PM6 calculations, gelation studies, SEM, AFM, WAXS, X-ray diffraction and EXAFS experiments.

AUTHOR INFORMATION

Corresponding Author

* E-mail: fernandg@uni-muenster.de

Present Addresses

[#] Departamento de Química Orgánica, Facultad de Ciencias, Universidad Autónoma de Madrid, 28049 Madrid, Spain.

[§] Organisch-Chemisches Institut, Westfälisch-Wilhelms Universität Münster, Corrensstraße, 40, 48149 Münster, Germany.

Author Contributions

All authors contributed equally.

Funding Sources

We thank the Humboldt Foundation (Sofja Kovalevskaja Award) and the Brazilian agencies CAPES (A061_2013) and CNPq (305082/2013-2) for financial support.

ACKNOWLEDGMENT

We thank Prof. Frank Würthner for helpful discussions and Dr. David Schmidt for crystal structure analysis.

REFERENCES

1. Yang, L.; Tan, X.; Wang, Z.; Zhang, X. Supramolecular Polymers: Historical Development, Preparation, Characterization, and Functions. *Chem. Rev.* **2015**, 115, 7196-7239.
2. Wei, P.; Yan, X.; Huang, F. Supramolecular polymers constructed by orthogonal self-assembly based on host–guest and metal–ligand interactions. *Chem. Soc. Rev.* **2015**, 44, 815-832.
3. Kulkarni, C.; Balasubramanian, S.; George, S. J. What Molecular Features Govern the Mechanism of Supramolecular Polymerization?. *ChemPhysChem.* **2013**, 14, 661-673.
4. De Greef, T. F. A.; Smulders, M. M. J.; Wolffs, M.; Schenning, A. P. H. J.; Sijbesma, R. P.; Meijer, E. W. Supramolecular Polymerization. *Chem. Rev*. **2009**, 109, 5687-5754.
5. Würthner, F.; Saha-Möller, C. R.; Fimmel, B.; Ogi, S.; Leowanawat, P.; Schmidt, D. Perylene Bisimide Dye Assemblies as Archetype Functional Supramolecular Materials. *Chem. Rev.* **2015**, 10.1021/acs.chemrev.5b00188S.
6. Yagai, S. Supramolecularly Engineered Functional π-Assemblies Based on Complementary Hydrogen-Bonding Interactions. *Bull. Chem. Soc. Jpn.* **2015**, 88, 28-58.
7. Schill, J.; Schenning, A. P. H. J.; Brunsveld, L. Self-Assembled Fluorescent Nanoparticles from π-Conjugated Small Molecules: En Route to Biological Applications. *Macromol. Rapid Commun.* **2015**, 36, 1306-1321.

8. Tayi, A. S.; Kaeser, A.; Matsumoto, M.; Aida, T.; Stupp, S. I. Supramolecular ferroelectrics. *Nature Chem.* **2015**, 7, 281-294.
9. Müllen, K. Evolution of Graphene Molecules: Structural and Functional Complexity as Driving Forces behind Nanoscience. *ACS Nano*, **2014**, 8, 6531-6541.
10. Babu, S. S.; Praveen V. K.; Ajayaghosh, A. Functional π-Gelators and Their Applications. *Chem. Rev.* **2014**, 114, 1973-2129.
11. Li, W.; Kim, Y.; Li, J.; Lee, M. Dynamic self-assembly of coordination polymers in aqueous solution. Soft *Matter.* **2014**, 10, 5231-5242;
12. Molla, M. R.; Ghosh, S. Aqueous self-assembly of chromophore-conjugated amphiphiles. *Phys. Chem. Chem. Phys.* **2014**, 16, 26672-26683.
13. Das, A.; Ghosh, S. Supramolecular Assemblies by Charge-Transfer Interactions between Donor and Acceptor Chromophores. *Angew. Chem. Int. Ed.* **2014**, 53, 2038-2054.
14. Boekhoven J.; Stupp, S. I. 25th Anniversary Article: Supramolecular Materials for Regenerative Medicine. *Adv. Mater.* **2014**, 26, 1642-1659.
15. Korevaar, P. A.; De Greef T. F. A.; Meijer, E. W. Pathway Complexity in π-Conjugated Materials. *Chem. Mater.* **2014**, 26, 576-586.
16. Rybtchinski, B. Aqueous Supramolecular Polymers Based on Aromatic Amphiphiles: Rational Design, Complexity, and Functional Materials. *Adv. Polym. Sci.* **2013**, 262, 363-387.
17. Busseron, E.; Ruff, Y.; Moulin, E.; Giuseppone, N. Supramolecular self-assemblies as functional nanomaterials. *Nanoscale*, **2013**, 5, 7098-7140.
18. Aida, T.; Meijer E. W.; Stupp, S. I. Functional Supramolecular Polymers. *Science* **2012**, 335, 813-817.
19. Rest, C.; Kandanelli R.; Fernández, G. Strategies to create hierarchical self-assembled structures via cooperative non-covalent interactions. *Chem. Soc. Rev.* **2015**, 44, 2543-2572.
20. Gonzalez-Rodriguez, D.; Schenning, A. P. H. J. Hydrogen-bonded Supramolecular π-Functional Materials *Chem. Mater.* **2011**, 23, 310-325.
21. Lok, C.-N.; Zou, T.; Zhang, J.-J.; Lin I. W.-S.; Che, C.-M. Controlled-Release Systems for Metal-Based Nanomedicine: Encapsulated/Self-Assembled Nanoparticles of Anticancer Gold(III)/Platinum(II) Complexes and Antimicrobial Silver Nanoparticles. Adv. *Mater.* **2014**, 26, 5550-5557.
22. Mauro, M.; Aliprandi, A.; Septiadi, D.; Kehra, N. S.; De Cola, L. *When self-assembly meets biology: luminescent platinum complexes for imaging applications. Chem. Soc. Rev.* **2014**, 43, 4144-4166.
23. Wang W.; Yang, H.-B. Linear neutral platinum–acetylide moiety: beyond the links. *Chem. Commun*. **2014**, 50, 5171-5186.
24. Lanigan N.; Wang, X. S. Supramolecular chemistry of metal complexes in solution. *Chem. Commun.* **2013**, 49, 8133-8144.
25. Tam A. Y.-Y.; Yam, V. W.-W. Recent advances in metallogels. *Chem. Soc. Rev.* **2013**, 42, 1540-1567.
26. Wong K. M.-C.; Yam, V. W.-W. Self-Assembly of Luminescent Alkynylplatinum(II) Terpyridyl Complexes: Modulation of Photophysical Properties through Aggregation Behavior. *Acc. Chem. Res.* **2011**, 44, 424-434.
27. Eryazici, I.; Moorefield C. N.; Newkome, G. R. Square-Planar Pd(II), Pt(II), and Au(III) Terpyridine Complexes: Their Syntheses, Physical Properties, Supramolecular Constructs, and Biomedical Activities. *Chem. Rev.* **2008**, 108, 1834-1895.
28. Williams, J. A. G. Photochemistry and Photophysics of Coordination Compounds: Platinum. *Top. Curr. Chem.* **2007**, 281, 205-268.
29. Lai S. W.; Che, C. M. Luminescent Cyclometalated Diimine Platinum(II) Complexes: Photophysical Studies and Applications. *Top. Curr. Chem.* **2004**, 241, 27-63.
30. Kimizuka, N. Towards Self-Assembling Inorganic Molecular Wires. *Adv. Mater.* **2000**, 12, 1461-1463.
31. Yam, V. W.-W.; Au V. K.-M.; Leung, S. Y.-L. Light-Emitting Self-Assembled Materials Based on d8 and d10 Transition Metal Complexes. *Chem. Rev*. **2015**, 115, 7589-7728.
32. Allampally, N. K.; Daniliuc, C.-G.; Strassert C. A.; De Cola, L. Tuning the Structural and Photophysical Properties of Cationic Pt(II) Complexes Bearing Neutral Bis(triazolyl)pyridine Ligands. *Inorg. Chem.* **2015**, **54**, 1588-1596.
33. Tian, Y.-K.; Shi, Y.-G.; Yang, Z.-S.; Wang, F. Responsive Supramolecular Polymers Based on the Bis[alkynylplatinum(II)] Terpyridine Molecular Tweezer/Arene Recognition Motif. *Angew. Chem. Int. Ed*. **2014**, 53, 6090-6094.
34. Mauro, M.; Aliprandi, A.; Cebrián, C.; Wang, D.; Kübel C.; De Cola, L. Self-assembly of a neutral platinum(II) complex into highly emitting microcrystalline fibers through metallophilic interactions. *Chem. Commun.* **2014**, 50, 7269-7272.
35. Au-Yeung, H.-L.; Leung, S. Y.-L.; Tam A. Y.-Y.; Yam, V. W.-W.Transformable Nanostructures of Platinum-Containing Organosilane Hybrids: Non-covalent Self-Assembly of Polyhedral Oligomeric Silsesquioxanes Assisted by Pt···Pt and π–π Stacking Interactions of Alkynylplatinum(II) Terpyridine Moieties. *J. Am. Chem. Soc*. **2014**, 136, 17910-17913.
36. Leung, S. Y.-L.; Lam W. H.; Yam, V. W.-W. Dynamic scaffold of chiral binaphthol derivatives with the alkynylplatinum(II) terpyridine moiety. *Proc. Natl. Acad. Sci. U.S.A.*, **2013**, 110, 7986-7991.
37. Ng C.-F.; Chow, H.-F. A supramolecular ladder polymer prepared by hydrogen bonding-mediated self-assembly of a metallomacrocycle. *Chem. Commun.* **2015**, 51, 2349-2352.
38. Tian, Y.-J.; Meijer, E. W.; Wang, F. Cooperative self-assembly of platinum(II) acetylide complexes. *Chem. Commun*. **2013**, 49, 9197-9199.
39. Xu, X.-D.; Zhang, J.; Chen, L.-J.; Zhao, X.-L.; Wang, D.-X.; Yang, H.-B. Large-Scale Honeycomb Microstructures Constructed by Platinum–Acetylide Gelators through Supramolecular Self-Assembly. *Chem. Eur. J.* **2012**, 18, 1659-1667.
40. Krikorian, M.; Liu S.; Swager, T. M. Columnar Liquid Crystallinity and Mechanochromism in Cationic Platinum(II) Complexes. *J. Am. Chem. Soc.* **2014**, 136, 2952-2955.
41. Stengel, I.; Strassert, C. A.; De Cola, L.; Bäuerle, P. Tracking Intramolecular Interactions in Flexibly Linked Binuclear Platinum(II) Complexes. *Organometallics*, **2014**, 33, 1345-1355.
42. Chang, K.-C.; Lin, J.-L.; Shen, Y.-T.; Hung, C.-Y.; Chen, C.-Y.; Sun, S.-S. Synthesis and Photophysical Properties of Self-Assembled Metallogels of Platinum(II) Acetylide Complexes with Elaborate Long-Chain Pyridine-2,6-Dicarboxamides. *Chem. Eur. J*. **2012**, 18, 1312-1321.
43. Leung, S. Y.-L.; Lam, E. S.-H.; Lam, W. H.; Wong, K. M.-C.; Wong, W.-T.; Yam, V. W.-W. Luminescent Cyclometalated Alkynylplatinum(II) Complexes with a Tridentate Pyridine-Based N-Heterocyclic Carbene Ligand: Synthesis, Characterization, Electrochemistry, Photophysics,

and Computational Studies. *Chem. Eur. J.* **2013**, 19, 10360-10369.
44. Chan, A. K.-W.; Lam, E. S.-H.; Tam, A. Y.-Y.; Tsang, D. P.-K.; Lam, W. H.; Chan, M.-Y.; Wong, W.-T.; Yam, V. W.-W. Synthesis and Characterization of Luminescent Cyclometalated Platinum(II) Complexes of 1,3-Bis-Hetero-Azolylbenzenes with Tunable Color for Applications in Organic Light-Emitting Devices through Extension of π Conjugation by Variation of the Heteroatom. *Chem. Eur. J.* **2013**, 19, 13910-13924.
45. Kui, S. C.-F.; Hung, F. F.; Lai, S. L.; Yuen, M. Y.; Kwok, C. C.; Low, K. H.; Chui, S. S. Y.; Che, C.-M. Luminescent Organoplatinum(II) Complexes with Functionalized Cyclometalated C^N^C Ligands: Structures, Photophysical Properties, and Material Applications. *Chem. Eur. J.* **2012**, 18, 96-109.
46. Plasseraud, L.; Gonzalez Cuervo, L.; Guillon, D.; Süss-Fink, G.; Deschenaux, R.; Bruce, D. W.; Donnio, B. Hexacatenar liquid-crystalline complexes of palladium(II) and platinum(II) based on trialkoxystilbazole esters. *J. Mater. Chem*, **2002**, 12, 2653-2658.
47. Mongin, C.; Donnio, B.; Bruce, D. W. On the Formation of the Thermotropic Cubic Phase: Insights from Monoacetylide Complexes of Pt(II). *J. Am. Chem. Soc*. **2001**, 123, 8426-8427.
48. Donnio B.; Bruce, D. W. Liquid-crystalline complexes of palladium(II) and platinum(II) with di- and tri-alkoxystilbazoles: ligand control of mesomorphism. *J. Chem. Soc*. *Dalton Trans*. **1997**, 2745-2755.
49. Chen, M.; Wei, C.; Wu, X.; Khan, M.; Huang, N.; Zhang, G.; Li, L. Metallogels Self-Assembled from Linear Rod-Like Platinum Complexes: Influence of the Linkage. *Chem. Eur. J*. **2015**, 21, 4213-4217.
50. Chen, M.; Wei, C.; Tao, J.; Wu, X.; Huang, N.; Zhang, G.; Li, L. Supramolecular Polymers Self-Assembled from trans-Bis(pyridine) Dichloropalladium(II) and Platinum(II) Complexes. *Chem. Eur. J*. **2014**, 20, 2812-2818.
51. Stepanenko, V.; Kandanelli, R.; Uemura, S.; Würthner, F.; Fernández, G. Concentration-dependent rhombitrihexagonal tiling patterns at the liquid/solid interface. *Chem. Sci.* **2015**, 6, 5853-5858.
52. Rest, C.; Mayoral, M. J.; Fucke, K.; Schellheimer, J.; Stepanenko, V.; Fernández, G. Self-Assembly and (Hydro) gelation Triggered by Cooperative π–π and Unconventional C-H··· X Hydrogen Bonding Interactions. *Angew. Chem. Int. Ed.* **2014**, 53, 700-705.
53. Mayoral, M. J.; Rest, C.; Stepanenko, V.; Schellheimer, J.; Albuquerque, R. Q.; Fernández, G. Cooperative Supramolecular Polymerization Driven by Metallophilic Pd··· Pd Interactions. *J. Am. Chem. Soc.* **2013**, 135, 2148-2151.
54. Zhao, Y.; Roberts, G.; Greenough, S.; Farrer, N.; Paterson, M.; Powell, W.; Stavros, V.; Sadler, P. Two-Photon-Activated Ligand Exchange in Platinum(II) Complexes. *Angew. Chem. Int. Ed*. **2012**, 51, 11263-11266.
55. Markvoort, A. J.; ten Eikelder, H. M.; Hilbers, P. A.; de Greef, T. F. A.; Meijer, E. W. Theoretical models of nonlinear effects in two-component cooperative supramolecular copolymerizations. *Nat. Commun.* **2011**, 2, 509.
56. Ten Eikelder, H. M. M.; Markvoort, A. J.; de Greef, T. F. A.; Hilbers, P. A. J. An Equilibrium Model for Chiral Amplification in Supramolecular Polymers. *J. Phys. Chem. B*, **2012**, 116, 5291-5301.
57. Řezáč, J.; Hobza, P. Advanced Corrections of Hydrogen Bonding and Dispersion for Semiempirical Quantum Mechanical Methods. *J. Chem. Theory Comput.* **2012**, 8, 141-151.
58. MOPAC2012, Stewart, J. P. Computational Chemistry, Version 15.180M, web: HTTP://OpenMOPAC.net.
59. Maia, J. D. C.; Carvalho, G. A. U.; Mangueira, Jr. C. P.; Santana, S. R.; Cabral, L. A. F.; Rocha, G. B. GPU Linear Algebra Libraries and GPGPU Programming for Accelerating MOPAC Semiempirical Quantum Chemistry Calculations *J. Chem. Theory Comput*. **2012**, 8, 3072-3081.
60. Johnstone, T. C.; Lippard, S. J. The Chiral Potential of Phenanthriplatin and Its Influence on Guanine Binding. *J. Am. Chem. Soc*. **2014**, 136, 2126–2134.

Insert Table of Contents artwork here